Investigation of Monitoring Systems for Resistance Spot Welding

A variety of sensor systems were studied to find which one provided the most information about nugget formation

BY C.-S. CHIEN AND E. KANNATEY-ASIBU, JR.

ABSTRACT. Although many different sensors have been developed for monitoring the resistance spot welding (RSW) process, no single sensor has been found to be capable of reliably detecting all defects associated with the process. A number of sensor systems are considered to hold promise of providing information about the process. In this paper, an investigation of various sensor systems for RSW is presented and the signals are analyzed and correlated with nugget formation and growth. These include a fiber-optic displacement sensor, an acoustic emission sensor, a force transducer, and the current and voltage measurements, which are set up to simultaneously monitor the welding process. Of these sensor systems, force signals are found to provide the most information on nugget formation.

Introduction

Resistance spot welding (RSW) involves joining sheets of material by simultaneous application of pressure and current. Resistance to the flow of current at the interface between the two pieces results in material close to the interface being heated to a temperature beyond the melting point. A nugget thus forms to join the two materials. Several sensors have been developed for monitoring the resistance welding process. These include measurement of the power input by using the electrical signals such as tip voltage, current, and dynamic resistance. This is based on the assumption that most of the resistance variations during the welding process occur at the faying interface and, thus, the power input monitored would be proportional to the heat generated at the faying interface. However, Ref. 1 showed when welding galvanized steel, most of the resistance variations during the process occur at the electrode-sheet interface, not at the faying interface. Instead of reflecting the resistance change at the faying interface, monitoring the dynamic resistance during welding of galvanized steel would be more indicative of electrode wear.

Other techniques involve monitoring the mechanical response of the welding process, such as force, displacement, and acoustic emission (AE). Since these parameters are the direct result of the complex reactions of the welding process, more information can generally be obtained by monitoring these signals. The electrode force is automatically adjusted by designing the welding head so that any reverse movement of the electrode after it has been brought into contact with the workpieces is controlled by hydraulic brake calipers (Ref. 2). This suppresses weld growth by increasing the electrode force automatically if the weld is growing too fast. The electrode force also has been monitored and adjusted (Ref. 3), but only to ensure the applied load is within a predetermined range. The dynamic force measured by a strain gauge-based transducer is often contaminated by the strong magnetic field associated with the welding cycles. Measuring force away from the electrode tips to minimize magnetic interference gives different results from the force actually experienced at the electrode tips due to the moving mass of the welding head (Ref. 1). It is believed measuring dynamic force close to the electrode tips would be a better signal source in applying to quality control of the high-volume production line. It has also been shown the force signals are useful in expulsion detection (Ref. 4).

Electrode displacement, which gives good indication of thermal expansion, melting, and expulsion, has proven to be a particularly useful signal to monitor. The linear variable differential transformer (LVDT) is the most commonly used device for extracting electrode displacement in the RSW process. A number of control systems have been developed based on maximum electrode displacement or its changing rate (Refs. 5–10). However, its intrusiveness has limited it only to pedestal welding machines. In Ref. 11, the electrode displacement was measured using a fiber-optic sensor. The results clearly showed the nugget grows with each current half cycle. Such precise measurement should enable more precise nugget control to be achieved.

Acoustic emission, which is capable of detecting the dynamic, real-time response of processes, has also been investigated. In Ref. 12, AE from postweld cracking was used as an indication of weld quality. Acoustic emission due to expulsion has been used as a control limit (Ref. 13).

The objective of this research is to investigate and compare a number of sensor monitoring systems that provide real-time information of nugget formation and growth for RSW. Acoustic emission, electrode displacement, force, and dynamic resistance will be investigated for correlation with weld formation. Improved sensing techniques on each parameter are also investigated. In the next section, sensing methods and data acquisition are presented, followed in subsequent sections by data analysis and results and discussion.

KEY WORDS

Acoustic Emission Sensor
Current
Fiber-Optic Displacement Sensor
Force Transducer
Resistance Spot Welding
Voltage

Sensing Methods and Data Acquisition

Different methods of measuring weld voltage, current, electrode displacement, and force were evaluated in this study. A

C.-S. CHIEN is a Graduate Student and E. KANNATEY-ASIBU, JR., is a Professor in the Dept. of Mechanical of Engineering, The University of Michigan, Ann Arbor, Mich.

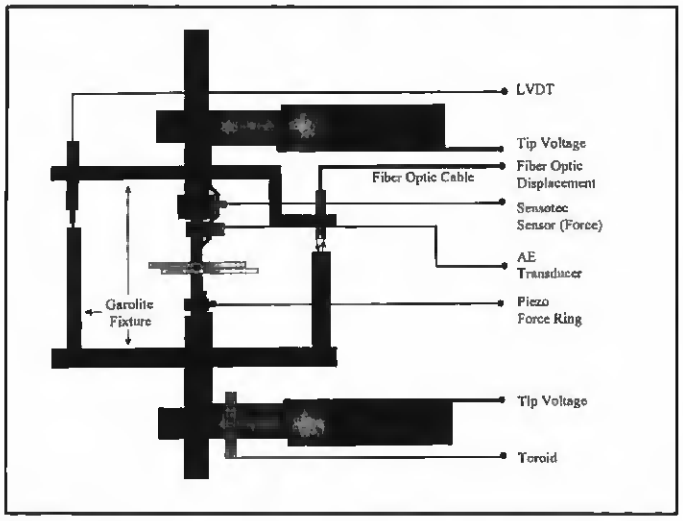

Fig. 1 — Instrumentation configuration showing the signals used for this study.

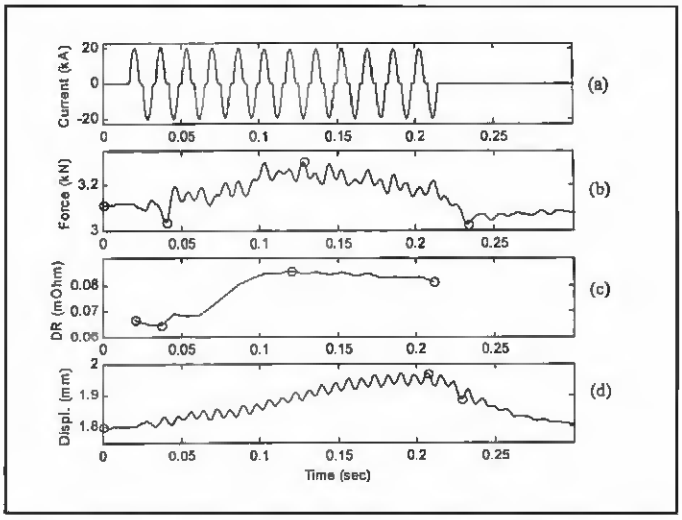

Fig. 2 — Typical signals of current, electrode force, dynamic resistance, and optical electrode displacement for 0.8-mm hot-dipped galvanized steel. Welding current was 12.7 kA RMS.

schematic of the instrumentation configuration is shown in Fig. 1. The welding machine used for this study is a Taylor Winfield pedestal machine, with 75-KVA capacity. Two commonly used methods of measuring current are studied. One involves using a toroid to measure the induced voltage and then integrating it to provide an indirect measurement of current. By hanging a toroid in the electrode arm with a fixture to keep it in the same position, variations in the position and orientation are minimized. The other method uses a Hall effect current sensor that measures the voltage across a semiconductor due to magnetic fields and thus is also sensitive to variation in orientation and position. More recent Hall effect sensors are less sensitive to orientation. In a 360-deg rotational test on two different pedestal welding machines, the new Hall effect sensor exhibited readings with less than 0.5% deviation.

A voltage correcting method (Ref. 14) was used for voltage measurement in the setup. The voltage across the workpiece was measured by routing two leads from the electrode tips along the welding machine arms to the data acquisition system for consistent measurement. The voltage signals were then corrected by canceling out the induced voltage using the signals obtained from the toroid.

Two methods of measuring the dynamic force near the electrode tips were investigated. One used a piezoelectric force ring and the other used a strain gauge-based force transducer. The force measured with the piezoelectric ring showed a decaying trend during the welding cycles, which might have been caused by the high magnetic field. Further investigation is needed to obtain accurate and uncorrupted force signals near the electrode tips using a piezoelectric transducer. For the strain gauge-type transducer, the output of the strain gauge is of the order of milivolts and thus is easily corrupted by the magnetic interference. An adaptive noise cancellation scheme (Ref. 4), which adaptively subtracts magnetic noise from a reference signal (the toroid output) to improve signal-to-noise ratio, was implemented in this study.

A fiber-optic displacement transducer (Ref. 11) and an LVDT setup to measure the electrode displacement are shown in Fig. 1. By using a fiber-optic cable to transmit and receive light to and from a target surface, displacement can be measured remotely without any electronic component close to the welding area, thus minimizing the chance of magnetic interference. The other advantage of the fiber-optic displacement sensor is the fact it is noncontact. The displacement jump within each half cycle can be accurately measured and not filtered out as in the case of LVDT measurement.

Acoustic emission is capable of real-time monitoring of some physical phenomena such as plastic deformation, cracking, melting, and martensitic transformation. To correlate AE signals to the onset of melting and nugget formation, the transducer needs to be located closer to the electrode tip. Mounting the transducer on the upper electrode shank (Fig. 1) was found to provide adequate information. AE during the welding cycles is acquired by using a data acquisition card that can simultaneously sample four channels at 5 MHz. A wire coil is positioned near the lower electrode arm to provide timing reference and trigger signal for viewing and measuring the AE signal. Acoustic emission signals can be collected continuously to the end of the weld cycles by using the hardware triggering provided by the data acquisition card. Signals are amplified through a preamplifier and an amplifier with a total gain of 50 dB.

The ten channels of data — current (two), voltage (two), displacement (two), force (two), AE RMS, toroid voltage — were sampled using a 12-bit data acquisition system. All the channels were sampled at 20 kHz each, except for the AE signal, which was sampled at 3 MHz and then digitally high-pass filtered at 100 kHz. Dynamic information was obtained for hot-dip galvanized steel. The experimental data is analyzed in the next section.

Data Analysis

Having acquired the individual signals, a better understanding of the process can be obtained by analyzing them together. Any feature observed in a single sensor's output can be applied to the multisensor system to further understand and confirm the measurement in the other signals.

Acoustic emission signals in the low frequency range tend to be of a much higher magnitude than the high-frequency signals, and the latter attenuate much more quickly. Thus, AE signals obtained at farther locations contain mostly low-frequency signals, while those obtained with the transducer near to the source contained both lower- and higher-frequency signals. Analysis of the raw AE signals as well as the spectrum and RMS values revealed no specific correlation between AE signals and nugget formation. Total AE counts beyond a threshold during welding cycles did not indicate nugget size as shown in earlier research.

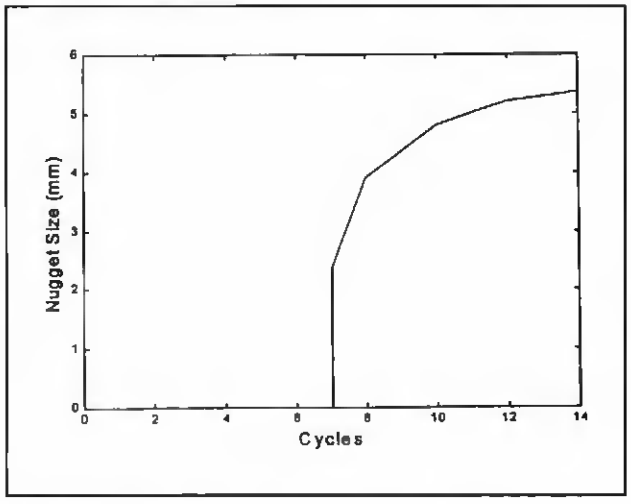

Fig. 3 — Nugget growth curve under the following welding conditions: current at 10.8-kA RMS, force at 3.05 kN before current initiation, with electrode tip size 6 mm.

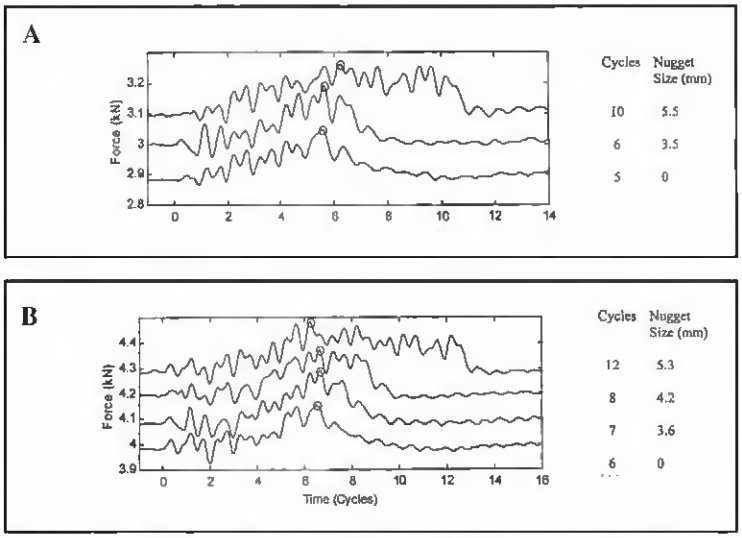

Fig. 4 — Variation of force signals with welding time. For ease of comparison, force data sets are shifted up and down from the starting force. A — Starting force, 3 kN; current applied, 12.1 kA; B — starting force, 4.1 kN; current applied, 12.3 kA

The electrode force signal was processed using the adaptive noise cancellation method (Ref. 4) at 5 kHz. The dynamic resistance was calculated only at the peak current and its corresponding tip voltage due to the fact the current changing rate is zero at this peak; hence, the induced voltage is minimized. Thus, each cycle is represented by two points and is available only during the welding cycles. The current, force, dynamic resistance, and optical displacement measurements are presented for a hot-dipped galvanized steel in Fig. 2. In general, the current data provides information on the time reference of current firing or ending in each half cycle, in addition to the input current level. Dynamic resistance provides most information on the electrode/sheet interface rather than the faying interface. The optical displacement provides dynamic expansion within each half current cycle due to the interaction of thermal expansion and applied electrode force. The force data ensures the applied force before welding current begins as well as its dynamic change within each half cycle. Force signals during the welding cycles are often overlooked due to the high magnetic interference. The other reason is machine characteristics such as arm stiffness and the way it supplies pressure vary with welding machine type. The results are discussed in the next section.

Results and Discussion

Mechanical systems generally have a response time. This can be seen from Fig. 2, as the force and displacement signals lag the current signal. From the experimental force data shown in Fig. 2B, the first point marked is the initial force level just before current is applied. The second point marked dips further with higher current application. This relates to burning of the interface coating. The third point marked represents peak force during the welding cycles. Even though electrode displacement still keeps increasing, it is believed the overall stiffness of the sheet metal between the electrodes starts to decrease at this point. Experiments under various loads were undertaken to investigate this phenomenon and the results are discussed later. This peak force does not necessarily increase as the applied current increases. However, it peaks earlier as the applied current increases, other welding conditions being the same. The fourth point correlates to the sudden drop of the electrode immediately after the current is cut off. The slope of this drop increases with higher current application. The difference between this point and the peak force is analogous to the peak force gain discussed in a later section.

The general dynamic resistance curve also has four points marked as shown in Fig. 2C. The first point is the resistance at the first peak current half cycle. The second point, which corresponds to the lowest resistance, denotes complete melting of the zinc coating. The third point is the peak resistance. The rate of increase from the second to the third point is often used as an indication of the overall temperature increase within sheet metals. The relative time from the third to the fourth point, which is the resistance at the end cycle, is mostly used as an indication of a good size weld (Ref. 1).

From the displacement signal measured by the fiber-optic sensor shown in Fig. 2D, the first point marked shows the initial position before current is applied. The second point corresponds to the peak electrode position during the welding cycles. The third point denotes the sudden drop right after the current is cut off. The slope of this drop increases with higher current application, similar to the fourth point marked in the force signal.

The initial nugget is usually formed within a period of one cycle under a typical welding schedule. A typical nugget growth curve (Fig. 3) shows the nugget quickly reaches a certain size within one cycle, then gradually increases in size at a decreasing rate. Initial melting for a specific set of welding conditions was obtained by performing a number of welds and varying the welding cycles one at a time. After each weld, the coupon was peeled to check nugget formation.

The sudden jump in nugget size evident in Fig. 3 can be detected using the force signals. Force measurement for various welding cycles under two different electrode loads is shown in Fig. 4. It is observed the force starts to decrease in magnitude after the nugget begins to form and keeps decreasing with subsequent welding cycles, even though electrode displacement continues to increase as a result of thermal expansion. This decrease in force is considered to be due to a reduction in overall stiffness of the workpiece between the electrodes. Table 1 shows Young's modulus and bulk modulus values at select temperatures (Ref. 15). Both Young's modulus and the bulk modulus decrease substantially as temperature increases from 300 to 1478 K. The bulk modulus of liquid iron at its triple point is 69.9 GPa (Ref. 16). The sharp decrease in the bulk modulus after melting results in the decrease in force as more material melts. The time at which the force reaches its

Table 1 — Elastic Moduli at Various Temperatures: Low Carbon Steel S10C (Ref. 15)

Temperature (K)	300	1478
Young's Modulus (GPa)	210	110
Bulk Modulus[a] (GPa)	165	129

(a) Liquid iron at its triple point has a bulk modulus of 69.9 GPa (Ref. 16).

peak relative to the current cut-off can thus be used as an indication of weld formation. Although it is good to know when the nugget starts to form during the welding process, it is more desirable to make a weld with a good nugget size. To develop a relationship between force peak and its subsequent force drop as the basis for determining when a nugget of acceptable size forms, further experiments were undertaken.

Sixty welds were randomly made using various conditions as shown in Table 2 with force values ranging from 2.1 to 4.9 kN, current from 8.6 to 14.6 kA, and welding cycles from 4 to 14 cycles. Results were processed by determining the initial force level before the welding current started; the time peak force occurred and its level; and the predetermined welding time. Weld sizes were shown in Fig. 5 with the ratio of force gain at its peak to the applied electrode force level before applying welding, and the ratio of the time between the force peak and current cut-off to the predetermined welding time. From Fig. 5, good welds (nugget size larger than 4.5 mm), undersized welds (nugget size larger than 1 mm but smaller than 4.5 mm), and no welds (no nugget forms or nugget size is smaller than 1 mm) are well separable. Good welds are in the region of force ratio higher than 6% and time ratio higher than 11%, undersized welds are in the region of force ratio higher than 6% and time ratio lower than 11%, and no welds are in the region of force ratio lower than 6%, with the exception of one good weld that is 4.5 mm in the undersized weld region and one good weld and six undersized welds in the no-welds region. It is noted if the predetermined welding cycle is not long enough to reach the real force peak, a wrong force peak with a small force gain and high time ratio will be observed, which then leads to the higher time ratio of the no-weld region. For example, as Fig. 4 shows, the local peaks do not increase monotonically. If the predetermined current cycle ends at the fourth cycle, which is before the real force peak, then it would show a force peak before the last half current cycle and be in the undersized weld region instead of in the no-weld region.

Table 2 shows welding conditions, peeled nugget sizes, and calculated force and time ratios. From Table 2 and Fig. 5, weld size can be categorized by setting threshold values of both force and time ratios.

Additional experiments with applied force levels higher than 5 kN show the high applied force causes plastic deformation of the material well before the nugget forms, and thus decreases the force gain during welding. The decrease in force gain

Table 2 — Experiment Matrix and Results Based on Force Signals (Material: 0.8-mm Galvanized Steel)

Current (kA)	Cycles	Applied Force (kN)	Nugget Size (mm)	Peak Force Time to Current Cut over Predetermined Welding Time	Peak Force Gain over Applied Force
11.8	8	2.08	5.8	0.13	0.107
12.2	6	3.90	0	0.08	0.038
12.2	6	3.90	0	0.08	0.040
12.2	6	3.91	1.1	0.08	0.044
13.9	6	3.91	5.2	0.17	0.042
12.9	6	3.90	4.1	0.17	0.058
10.1	6	3.89	0	0.00	0.035
10.0	12	3.90	0	0.04	0.047
10.0	9	3.92	0	0.33	0.031
10.0	9	3.91	0	0.06	0.029
12.7	9	3.89	5.5	0.39	0.061
11.2	11	3.90	4	0.14	0.058
11.3	6	3.03	0	0.00	0.051
12.5	6	3.03	4.6	0.33	0.069
9.4	8	3.03	0	0.13	0.043
11.9	8	3.03	4.9	0.25	0.066
8.6	10	3.02	0	0.20	0.057
11.1	10	3.01	4.5	0.30	0.074
13.8	10	3.03	6.7	0.18	0.179
11.3	10	2.94	4.2	0.05	0.102
12.5	8	2.94	5	0.13	0.101
12.6	7	2.94	5	0.14	0.099
14.6	5	2.93	5.6	0.40	0.094
13.2	5	2.91	4.4	0.10	0.116
10.7	11	2.93	4	0.05	0.118
10.7	9	2.91	2.9	0.06	0.110
12.5	8	2.91	5.4	0.25	0.114
10.6	6	2.92	0	0.08	0.055
11.7	5	2.92	0	0.10	0.058
13.3	5	2.91	4.5	0.10	0.117
9.4	10	2.93	0	0.05	0.052
10.6	10	2.91	4.1	0.10	0.134
11.3	10	3.85	4	0.05	0.083
10.6	12	4.59	0	0.04	0.050
11.0	8	2.01	5	0.13	0.163
11.3	8	4.27	0.7	0.00	0.048
12.7	6	4.94	2.4	0.00	0.031
11.1	10	2.91	4.6	0.15	0.129
10.8	10	4.54	0	0.00	0.041
11.3	8	3.98	2.5	0.06	0.061
12.7	6	4.59	3.7	0.08	0.046
12.6	6	3.26	4.2	0.08	0.109
12.4	8	3.27	5.4	0.31	0.112
10.8	12	4.48	0	0.04	0.055
12.6	12	4.50	5.6	0.21	0.072
12.7	6	3.59	3.7	0.08	0.074
13.4	6	3.57	5	0.17	0.100
11.5	6	4.66	0	0.25	0.026
11.3	8	3.27	2.3	0.06	0.079
10.0	8	3.29	0	0.00	0.042
10.3	10	4.41	0	0.00	0.052
10.0	14	4.40	0	0.07	0.046
11.2	10	3.43	4.3	0.10	0.105
14.1	6	3.43	5.6	0.17	0.109
12.7	6	3.44	4.2	0.00	0.077
13.5	5	3.46	4.2	0.10	0.087
14.6	7	3.42	7	0.43	0.109
14.4	4	4.42	0	0.13	0.025
13.4	6	4.42	3.1	0.00	0.047
12.5	8	3.13	5.1	0.19	0.118

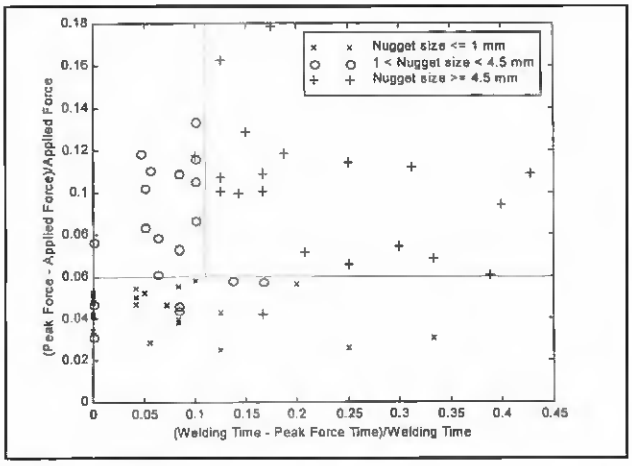

Fig. 5 — Weld sizes were shown with the ratio of force gain at its peak to the applied force level and the ratio of the time between the force peak and current cut-off to the predetermined welding time.

with high applied force will reduce the force ratio even for the good-sized welds, thus, high applied pressure is not desirable in this scheme.

Conclusions

A number of sensor systems were investigated for monitoring the resistance spot welding process. These included a fiber-optic displacement sensor, an acoustic emission sensor, a force transducer, and the current and voltage measurement. Signals were analyzed to correlate to the different stages of weld formation. Of the sensors investigated, the force signals clearly showed a decreasing trend upon the onset of melting and this can be used as an indication of weld formation. An early force peak with a threshold force gain and its subsequent force drop are essential to form a good-size weld. Monitoring the force signals should thus enable better weld quality to be achieved.

Acknowledgments

The authors are grateful to Doug Boomer at Alcan Aluminum Corp. USA for help with the instrumentation, Wei Li at the University of Michigan for providing the adaptive signal cancellation algorithm, and for the financial support of this work by the NIST Advanced Technology Program (NIST/ATP) through the Intelligent Resistance Welding Consortium.

References

1. Gedeon, S. A., Sorensen, C. D., Ulrich, K. T., and Eagar, T. W. 1987. Measurement of dynamic electrical and mechanical properties of resistance spot welds. *Welding Journal* 66(12): 378-s to 385-s.

2. Johnson, K. I. 1973. Resistance welding quality-control techniques. *Metal Construction and British Welding Journal* 5: 176–181.

3. Kuchar, N. R. 1982. A closed-loop control system for resistance spot welding. *ASME Winter Annual Meeting.*

4. Li, W. 1999. *Monitoring and Diagnosis of Resistance Spot Welding Process*. Ph.D. diss. Ann Arbor, Mich., The University of Michigan.

5. Waller, D. N., and Knowlson, P. M. 1965. Electrode separation applied to quality control in resistance welding. *Welding Journal* 44(12): 168-s to 174-s.

6. Cho, H. S., and Chun, D. W. 1985. A microprocessor-based electrode movement controller for spot weld quality assurance. *IEEE Transactions on Industrial Electronics* IE-32(3): 234–238.

7. Wood, R. T., Bauer, J. E., Bernstein, J., Czechowski, M. M. D'andrea, and Hogle, R. A. 1985. A closed-loop control system for three-phase resistance spot welding. *Welding Journal* 64(12): 26–30.

8. Stiebel, A., Ulmer, C., Kodrack, D., and Holmes, B. B. 1986. Monitoring and control of spot weld operations. *SAE International Congress and Exposition*. Detroit, Mich., #860579.

9. Chang, H. S., Cho, Y. J., Choi, S. G., and Cho, H. S. 1989. A proportional-integral controller for resistance spot welding using nugget expansion. *ASME Journal of Dynamic Systems, Measurement, and Control* 111: 332–336.

10. Haefner, K., Carey, B., Bernstein, B., and Overton, K. 1991. Real time adaptive spot welding control. *ASME Journal of Dynamic Systems, Measurement, and Control* 113: 104–112.

11. Chien, C. S., and Kannatey-Asibu Jr., E. 1998. Displacement measurement using a fiber-optic sensor in resistance spot welding. *Proceedings of the 5th International Conference on Trends in Welding Research*. Pine Mountain, Ga., pp. 622–627.

12. Notvest, K. R. 1974. Acoustic Emission Spot Welding Controller. U.S. Patent No. 3,824,377.

13. Vahaviolos, S. J. 1981. Adaptive spot weld feedback control loop via acoustic emission. *Material Evaluation*, Vol. 10, pp. 1057–1080.

14. Boomer, D. 1996. Private communication.

15. Fukuhara, M., and Sanpei, A. 1993. Elastic moduli and internal friction of low carbon and stainless steel as a function of temperature. *Iron and Steel Institute of Japan International* 33(4): 508–512.

16. Iida, T., and Guthrie, R. I. L. 1988. *The Physical Properties of Liquid Metals*. Oxford: Clarendon Press, p. 122.